Kaohsiung Journal of Medical Sciences (2013) 29, 246–253

Available online at www.sciencedirect.com

SciVerse ScienceDirect

journal homepage: http://www.kjms-online.com

ORIGINAL ARTICLE

In vivo magnetic resonance imaging of mice liver tumors using a new gadolinium-based contrast agent

Shih-Hsien Chen [a,b], Yu-Ting Kuo [b,c], Tian-Lu Cheng [d], Chiao-Yun Chen [b,c], Yen-Yu Chiu [b], Jui-Jen Lai [b], Chih-Ching Chang [b], Twei-Shiun Jaw [b,c], Yun-Ming Wang [e], Gin-Chung Liu [b,c,*]

[a] *Graduate Institute of Medicine, College of Medicine, Kaohsiung Medical University, Kaohsiung, Taiwan*
[b] *Department of Medical Imaging, Kaohsiung Medical University Hospital, Kaohsiung, Taiwan*
[c] *Department of Radiology, Faculty of Medicine, College of Medicine, Kaohsiung Medical University, Kaohsiung, Taiwan*
[d] *Faculty of Biomedical Science and Environmental Biology, College of Life Sciences, Kaohsiung Medical University, Kaohsiung, Taiwan*
[e] *Department of Biological Sciences and Technology, National Chiao-Tung University, Hsinchu, Taiwan*

Received 16 March 2012; accepted 24 April 2012
Available online 13 February 2013

KEYWORDS
Contrast;
β-glucuronidase;
Mouse liver;
MRI

Abstract We compared the enhancement effect between a newly synthesized tissue-specific contrast agent, [Gd-DOTA-FPβG], and a commercially available agent, $[Gd(DOTA)]^-$, in a murine model of liver tumor using a clinical magnetic resonance imaging scanner. The colon cancer cell lines with and without β-glucuronidase (βG) expression were implanted into the liver of mice. Self-synthesized gadolinium-based magnetic resonance contrast agent, [Gd(DOTA-FPβG)], was administered to measure enhancement on magnetic resonance images using a commercially available agent, $[Gd(DOTA)]^-$, as control in a clinical 3.0 tesla (T) magnetic resonance scanner. *In vivo* fluorescence imaging and histopathology of the liver were also performed to compare and correlate with the magnetic resonance studies. The *in vivo* fluorescence imaging failed to depict a sufficiently intense signal for liver or liver tumor of mice without exposure of the liver following an incision on the abdominal wall. The tissue-specific magnetic resonance agent, [Gd(DOTA-FPβG)], caused significantly stronger enhancement in tumors expressing βG (CT26/mβG-eB7) than in tumors not expressing βG (CT26) ($p < 0.05$). In the magnetic resonance imaging studies using control agent $[Gd(DOTA)]^-$, the tumors with and without βG expression depicted no significant difference in enhancement on the T1-weighted images. The [Gd(DOTA-FPβG)] also provided significantly more contrast uptake in the CT26/mβG-eB7 tumor than in the normal liver parenchyma, whereas the

* Corresponding author. Department of Medical Imaging, Kaohsiung Medical University Hospital, 100 Tzyou 1st Road, Kaohsiung 807, Taiwan.
E-mail address: gcliu@kmu.edu.tw (G.-C. Liu).

http://dx.doi.org/10.1016/j.kjms.2012.09.002

[Gd(DOTA)]$^-$ did not. This study confirms that better contrast enhancement can be readily detected *in vivo* by the use of a tissue-specific magnetic resonance contrast agent to target tumor cells with specific biomarkers in a clinical magnetic resonance imaging scanner.

Introduction

Several methods have been used to detect and assess hepatic tumors in current clinical practice. These include imaging studies [1,2], titration of tumor markers [3,4], and histopathology. Imaging methods usually provide a noninvasive *in vivo* opportunity to detect and to stage tumors. If a lesion does not have inherited tissue contrast, which can be detectable on certain imaging modalities, nonspecific contrast agents are usually needed to contrast the tumor and surrounding normal tissue. Examples are iodinated contrast agents for computed tomography, gadolinium-based agents for magnetic resonance imaging (MRI), or microbubble agents for ultrasonography. However, from a molecular point of view, most of these methods are only able to detect relatively late-staged, large-sized tumors. To detect and track tumors earlier, researchers are attempting to develop various types of tissue-specific contrast agents for different imaging strategies. These contrast agents can target tumor cells, with the result that the sensitivity and specificity of tumor detection improves [5–8]. To achieve this purpose, a significant amount of the contrast agent should have affinity with tumor cells, and be readily detected by *in vivo* imaging methods.

Certain biomarkers on tumor cells have been identified, and some of these have also been investigated for this particular purpose. One of these specific receptors on tumor cells is β-glucuronidase (βG), an enzyme that exists generally in cell microsomes (endoplasmic reticulum) and lysosomes [9]. Its concentration is low in the human serum and the extracellular substance of normal tissue [10]. However, in previous research, high βG expression on cell membranes of some tumors has been found [11]. Moreover, βG expression can also affect tumor biology, such as metastasis and invasiveness of tumors [11].

Molecular imaging studies using βG as a biomarker have been done. In former research studies, optical images such as fluorescence or luminescence were used to track subcutaneous tumors of small animals [12]. These experiments have succeeded in detecting tumors as well as monitoring the response to tumor treatments [13]. However, due to limited penetration power, optical image techniques struggle to detect sufficient signals from the deep tissues and organs of large animals or humans. To overcome such limitations, many researchers have attempted to use different imaging technology, such as positron emission tomography (PET) [14], single-photon emission computed tomography (SPECT) [5,15,16] or magnetic resonance imaging (MRI) [17,18]. PET and SPECT have high sensitivity to detect and locate tumor tissue. They can also provide quantification of signal change, so that lesions may be detected and treatment response monitored. However, use of radioactive agents and relatively poor spatial resolution are disadvantages of nuclear medicine. Synthesis of tissue- or receptor-specific radiopharmaceutical agents is also not widely available in clinical settings. MRI provides excellent spatial resolution without use of ionizing radiation, and has already gained wide clinical application. However, current MRI with use of nonspecific extracellular contrast agents is still limited in sensitivity for detection of diseases down to the molecular level. Improved signal-to-noise ratio of MRI and synthesis of tissue-specific agents are obviously required.

The diagnosis of hepatic tumors, such as hepatocellular carcinoma (HCC), remains a challenge to healthcare systems worldwide, particularly in epidemic areas of chronic viral hepatitis B and C [19,20]. These malignant tumors are highly fatal. Patients with liver cirrhosis caused by chronic infection of hepatitis B virus, or hepatitis C virus, alcoholism, nonalcoholic steatohepatitis, and aflatoxin injury are at high risk. Early detection of small HCCs with imaging provides the best prognosis. However, current imaging technologies are still not sufficiently sensitive to detect small HCCs. According to a systemic review, regardless of tumor size, sensitivity measures for detecting HCCs with ultrasound, computed tomography (CT), and MRI are 60%, 68%, and 81%, respectively [21]. Sensitivity is even lower for HCCs smaller than 2 cm. According to a study using explanted liver as standard, sensitivity measures for ultrasound, CT, and MRI are only 21%, 40%, and 47%, respectively [22]. More sensitive and specific imaging strategies are undoubtedly highly desirable.

Based on the reasons previously discussed, we used a self-synthesized MRI contrast agent, ([Gd(DOTA-FPβG)]) (DOTA-FPβG = 1-(2-difluoromethyl-4-(1-(4,7,10-triscarboxymethyl (1,4,7,10-tetraazacyclodecyl))acetamido)phenyl)-β-D-glucopyronuronate) [23], to perform an *in vivo* MRI experiment in a murine model of liver tumor. This MRI contrast medium consists of a gadolinium (III) complex and an enzymatic moiety (2-difluoromethylphenyl-β-D-galactopyranose). It can depict significant T1 shortening effect when the tumor has βG expression. The βG enzyme anchored on tumor cell membrane can hydrolyze the contrast medium and remove the β-D-galactopyranose. This molecular process on the cell membrane of the tumor induces contrast enhancement on the T1-weighted MRI. It may produce significant contrast effects between tumors with and without βG, and also between tumors with βG and normal liver tissue.

This study is aimed to provide principal proof of this tracer design. We implanted the colon cancers of the mice that were with and without βG expression separately into different parts of the animal's liver. Both optical images and MRI were performed. To verify the effects of tissue-specific agents that we synthesized, the commercially available nonspecific macrocyclic gadolinium-based agent, [Gd(DOTA)]$^-$, which possesses similar chemical structures,

was used as control MRI contrast agent. We compared the results of these imaging scans, and made correlations with histology to evaluate the ability of these imaging technologies in the detection of tumors.

Methods

The culture of tumor cells and animal model setup

Animal experiments were performed in accordance with institute guidelines. The CT26/mβG-eB7 and CT26 murine colon carcinoma cells were cultured at 37°C in an atmosphere of 5% CO_2 incubator. They were grown in Dulbecco's Minimal Essential medium (DMEM) (Sigma, St. Louis, MO, USA) that was supplemented with 5% heat-inactivated bovine calf serum, 100 U/mL penicillin, 100 μg/mL streptomycin, and 2 mM/L glutamine. The culture medium was replaced twice a week. After the cells had grown to occupy approximately 70% of the Petri dish, the cells were collected and stained with trypan blue. The active cells must account for more than 90% of total cells. The concentration of tumor cells was adjusted to 10^7/mL. Six- to 8-week-old BALB/c mice, each weighing approximately 25—30 g, were purchased from the National Laboratory Animal Center, Taipei, Taiwan. 2×10^6 CT26/mβG-eB7 and 2×10^6 CT26 tumor cells were injected into the subcutaneous tissue of the right and left hind limb, respectively. Two to 3 weeks after the injection, the tumors had grown to a diameter of 10—15 mm, then they were removed surgically and implanted into additional BALB/c mice livers. The BALB/c mice were injected with 90 mg ketamine and 10 mg xylazine per kilogram of body weight into the peritoneal cavity for anesthesia. A 2-cm wound was made on the mice by a midline incision. The CT26/mβG-eB7 and CT26 tumors, each an approximately 1—2 mm diameter clump, were implanted in the right side and left side of the left lateral lobe liver of the BALB/c mice, respectively, and the muscle layers and skin were then sutured. After 7 days, the tumor growth extent of each mouse was confirmed by MRI.

In vivo fluorescence imaging of liver with CT26/mβG-eB7 and CT26 tumors

After 10—14 days of tumor implantation, the tumors in the liver had grown up to 5—10 mm in diameter. Each whole body image was obtained by performing a 10-second scan using the IVIS 50 optical imaging system (Caliper Life Sciences, Hopkinton, MA). Mice were anesthetized using 1% isoflurane, and then scanned before and after intravenous injection of fluorescein di-β-D-glucuronide (FDGlcU) (Invitrogen, Eugene, OR) every 5 minutes for 90 minutes. Each mouse was injected with 500 μg FDGlcU from the tail vein. The images were taken to measure the fluorescence signal intensity, and the curve of signal was drawn to analyze the signal changes.

In vivo MRI of liver with CT26/mβG-eB7 and CT26 tumors

Twelve BALB/c mice bearing CT26/mβG-eB7 and CT26 tumors 5—10 mm diameter on the right and left side of the left lateral lobe liver were established. The mice were anesthetized with 90 mg/kg ketamine and 10 mg/kg xylazine. Each mouse was placed in an animal coil in the prone position. MRI was performed using a 3T MRI scanner (Sigma; GE Medical Systems, Milwaukee, WI, USA). T2-weighted coronal fast-spin echo (FSE) (Repetition time (TR)/Echo time (TE) 3000/30 ms) and T1-weighted FSE (TR/TE 100/15 ms) axial images before and after intravenous injection of the contrast agent ([Gd(DOTA-FPβG)]) were obtained. After precontrast scanning, six mice were intravenously injected with 0.1 mmol/kg [Gd(DOTA)-FPβG] from the tail vein whereas the other six mice were intravenously injected with 0.1 mmol/kg $[Gd(DOTA)]^-$ (Dotarem, Guerbet, France) as a control group. Postcontrast scans were performed every 5 minutes for six subsequent scans. Scans were captured every 10 minutes until the 90-minute mark was reached. A glass cylinder of pure water was positioned adjacent to each mouse as a standard reference. The MRI signal intensity of liver tissue and both tumors within the liver were measured, and the curve of signal was drawn to analyze the signal changes.

Image analysis

The regions of interest from MRI of the tumors, liver tissue, and the water phantom were selected by the researcher. The signal intensity of each tumor and liver were normalized to enhancement ratio by dividing their mean target signal intensity by that of the water phantom (signal to noise ratio, SI/N). The enhancement percentage of the targets was calculated as:

$$\text{Enhancement}(\%) = ((\text{SI/N})\text{t} - (\text{SI/N})\text{pre})/(\text{SI/N})\text{pre} \times 100$$

The percentages of SI/N enhancement in different points in time were compared among different groups. The results were expressed as the mean ± standard deviation. The statistics were performed with the software GraphPad Prism (JMP 8, SAS Institute Inc, Cary, NC; Prism, GraphPad software Inc, La Jolla, CA, USA). The two-way analysis of variance using random effect model was used to compare the difference between groups. *Post hoc* comparison for enhancement at each point of time was also carried out when significant difference occurred. The p values that were below 0.05 were considered statistically significant.

Histologic analysis

After the MRI and fluorescent scanning, the tumors and liver tissues were excised and embedded into a frozen tissue embedding medium (Tissue-Tek, Sakura Finetek, Torrance, CA) in a −80°C refrigerator. Each tumor and liver tissue sample was then sectioned into two 10-μm slices. One section of tissue was stained for βG activity with the βG reporting gene staining kit (Sigma Diagnostics, St. Louis, MO) and counterstained with nuclear fast red. Other tissue sections were stained with a hematoxylin and eosin stain. Each section was examined using upright BX4 microscopy (Olympus, Melville, NY).

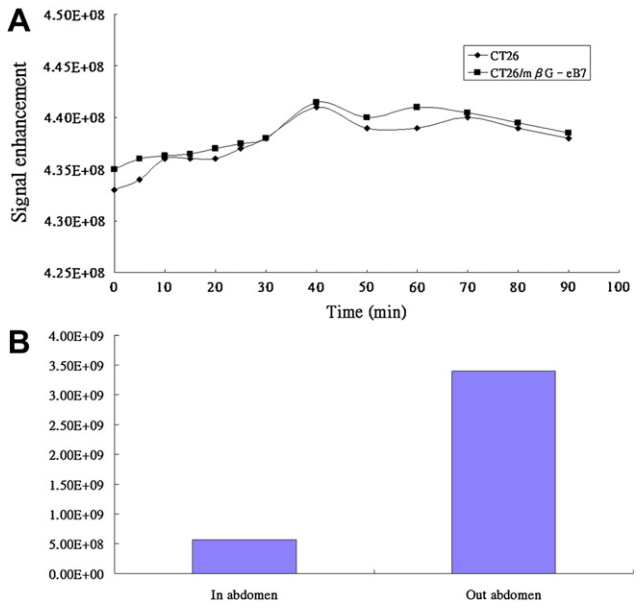

Figure 1. Time course curve, signal intensity of fluorescent images of CT26 and CT26/mβG-eB7. The overall signal before exposing liver is low. The signal intensity of fluorescence does not demonstrate significant difference between CT26/mβG-eB7(■) and CT26 tumors(◆). After the incision of the abdominal wall and exposure of the liver, the signal is significantly higher than that of the animal without exposure of liver at 35 minutes after the injection of fluorescent probes FDGlcU(B).

Results

In vivo fluorescence imaging of CT26/mβG-eB7 and CT26 tumors

No significant fluorescence signal was found from the images of all time periods selected (Fig. 1). During the last scan period, we made an incision into the abdomen of a mouse and exposed the liver tissue for a period of 35 minutes after the injection of fluorescent probes FDGlcU (Fig. 2A). Then, the image could be detected. There was a green fluorescence of fluorescein isothiocyanate (FITC) on the area of the right side of the liver lobe (Fig. 2B). The results indicated that the FDGlcU probe was actually hydrolyzed to FITC by βG enzyme in CT26/mβG-eB7 tumor, but fluorescence of FITC in liver tumors could not be detected because of the abdominal muscles and skin barrier.

In vivo MRI of liver with CT26/mβG-eB7 and CT26 tumors

As MRI of CT26/mβG-eB7 and the CT26 tumors in liver was performed, scans were performed on mice to obtain coronal section images with T2-weighted sequence. The size and position of tumors could be confirmed from the T2-weighted image. CT26/mβG-eB7 and CT26 tumors encountered similar distributions of contrast medium because they were both implanted in the left lateral lobe of the liver. The separation distance between tumors was more than 5 mm so that tumors would not fuse together (Fig. 3). The images of tumors and the liver after the intravenous injections of contrast medium [Gd(DOTA-FPβG)] showed stronger signal intensity in the area of the CT26/mβG-eB7 tumor within a period of 5 minutes. The signal enhancement was not present in the area of the CT26 tumor. The signals of CT26/mβG-eB7 tumors were higher than those of CT26 tumors 10 minutes after the injection of contrast agent (Fig. 4), and the appearance of enhancement remained until it reached 90 minutes. The highest signal in the average curve of CT26/mβG-eB7 tumors was observed 10 minutes after injection. It showed 25% enhancement more than the average signal of the CT26 tumors, and 20% more than an average signal of liver tissues (Fig. 5). The signals obtained from CT26/mβG-eB7 and CT26 tumors were significantly different ($p < 0.05$).

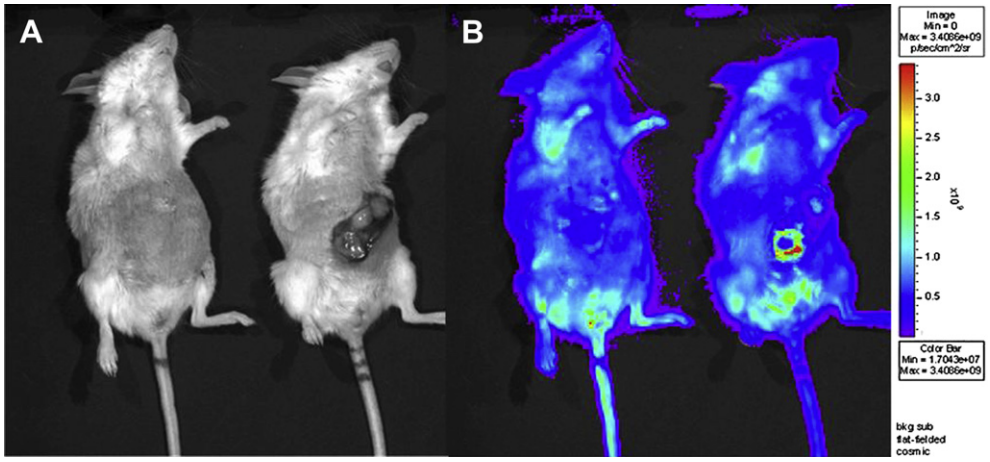

Figure 2. Fluorescent images of CT26 and CT26/mβG-eB7 before (left in A and B) and after (right in A and B) the excision of the abdominal wall. There was no significant signal from the liver tumor before the excision. The signals can be detected after the exposure of the liver. The CT26/mβG-eB7 tumor depicts a stronger fluorescent signal than the CT26 tumor after abdominal wall excision (right in B). There are some autofluorescent signals expressed on the hairs of the limbs and head.

Figure 3. Photograph of the excised CT26/mβG-eB7 and CT26 tumors in the left lateral lobe of the liver. No significant gross difference was seen between these two lesions.

MRI of CT26/mβG-eB7 and the CT26 tumors in the liver of the mice was performed with the commercially available nonspecific MRI contrast agent $[Gd(DOTA)]^-$. The apparent signal enhancement in the liver tissue was observed, but the signal intensities of CT26/mβG-eB7 and the CT26 tumors were inferior to those of the liver tissues (Fig. 6). The average signals of CT26/mβG-eB7 and CT26 tumors showed similar fluctuations along with time (Fig. 7). The signals obtained from CT26/mβG-eB7 and CT26 tumors were not significantly different ($p > 0.05$).

Histologic analysis and immune stain of tumors

To confirm the correlation between images and histologic analysis, BALB/c mice were sacrificed by excessive anesthesia, and the liver and tumors after MRI were excised. These tissues were embedded in the frozen tissue embedding medium and sectored into two 10-μm slices. The slices were stained with X-GlcA dyes: a βG reporting gene staining kit, and hematoxylin and eosin stain, respectively. Then, we compared the MRI scans and tissue sections. As shown in

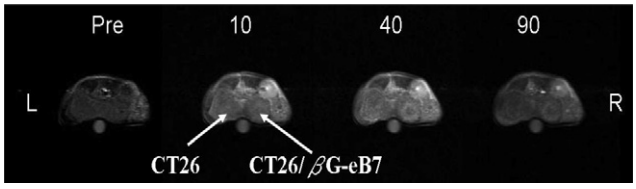

Figure 4. Gd-DOTA-FPβG enhanced T1-weighted MR images in mice. Pre = Pre-contrast image. The numbers indicate time (minutes) after intravenous administration of the contrast medium. The images show higher signal intensity in the CT26/mβG-eB7 tumor than in the CT26 tumor and liver from 10 minutes after the contrast agent, and the obvious difference remained constant until 90 minutes. As the time passed, the signal intensity in livers and CT26 tumors decreased. The signal intensity in the CT26/mβG-eB7 tumor remains higher than the other until the end of the scan.

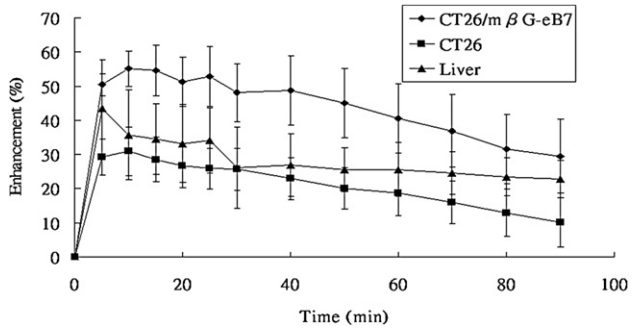

Figure 5. Time-enhancement change of tumors and livers after intravenous injections of contrast medium [Gd(DOTA-FPβG)]. The CT26/mβG-eB7 tumor shows a stronger signal intensity from 5 to 90 minutes. The highest average signal of the CT26/mβG-eB7 tumor was at 10 minutes. It was about 25% more enhanced than an average signal of the CT26 tumor, and 20% more than an average signal of liver tissues. The signals obtained from CT26/mβG-eB7 and CT26 tumors were statistically different ($p < 0.001$, $N = 6$).

Fig. 8, the slice showed CT26/mβG-eB7 tumor and liver tissues that were stained by hematoxylin and eosin (A and C), and stained by X-GlcA (B and D). The area of CT26/mβG-eB7 tumor was dyed with blue color because of the presence of βG enzyme in the tumor. The CT26 tumor and liver tissue were not stained blue due to the absence of βG enzyme in those tissues. The results of histology and MRI were consistent with the effects of the βG enzyme.

Discussion

In this study, we confirmed that the MRI contrast medium [Gd(DOTA-FPβG)] could depict tumors with βG expression in liver of a mouse model. This contrast medium is designed to target the βG of the tumor cells. The highly expressive βG enzyme of the tumor cells hydrolyzes the contrast medium and expresses a T_1 shortening effect. At the same time, the concentration on the tumor cell is also high enough to be detected by current MRI. In addition, we have also documented that this imaging strategy can not only detect tumors, but also differentiate tumors with and without certain biomarkers in a deep visceral organ *in vivo* by a noninvasive imaging modality, i.e., MRI, which has already been available in most current clinical settings.

In the fluorescence imaging experiment, the *in vivo* optical imaging system is unable to detect liver tumors

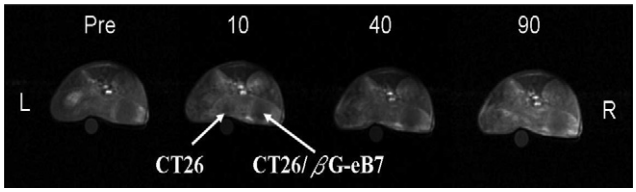

Figure 6. $[(Gd\text{-}DOTA)]^-$ enhanced T1-weighted MR images in mice. The numbers indicate time (minutes) after intravenous administration of contrast medium. Both tumors are relatively less enhanced than the liver. Pre = Pre-contrast image.

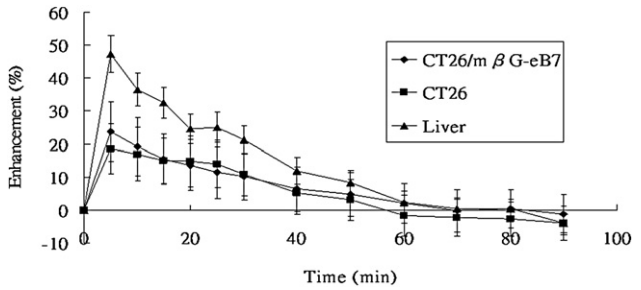

Figure 7. Time-enhancement curves of the tumors and livers after intravenous injections of contrast medium $[Gd(DOTA)]^-$. The signals of the CT26/mβG-eB7 and the CT26 tumors reveal no significant difference ($p = 0.67$, $N = 6$). Both were less enhanced than the liver.

reliably. The result is different from former fluorescence imaging of subcutaneous tumor studies. The fluorescence imaging system is able to detect the size and scope of a subcutaneous tumor clearly. The signals of the probe in images are strong and easily detected even in a small tumor. However, the penetration power of fluorescence is too weak to penetrate through thick muscle or tissue. This is why the received signal of the probe from the liver tumor is not as clear as that from the subcutaneous tumor in the *in vivo* optical imaging system. In our experiment, the signal could be depicted only when the liver tumor was removed from the abdomen by surgery.

We used the commercially available nonspecific extracellular contrast agent, $[Gd(DOTA)]^-$, as a control to compare the enhancement effect with the self-synthesized agent, [Gd(DOTA-FPβG)]. [Gd(DOTA-FPβG)] and $[Gd(DOTA)]^-$ both have the $[Gd(DOTA)]^-$ chelate with ring structure. The difference between the two contrast media is that [Gd(DOTA-FPβG)] has the functional structure of glucuronide base to be hydrolyzed by βG enzyme of the tumor, whereas $[Gd(DOTA)]^-$ does not. As the glucuronide base is removed from [Gd(DOTA-FPβG)], the surplus part of the agent binds with βG or the albumin and remains in the tumor tissue for a longer time period. An inference can be confirmed from the time-enhancement graph in the signal of tumors in the liver with these two contrast media. Our results showed that the distribution and the enhancement of extracellular contrast medium in the liver tissues and CT26/mβG-eB7, and CT26 tumors are not statistically different. This also indicates that the extracellular space and vascular distribution of CT26/mβG-eB7 and the CT26 tumors are similar [24]. A different result for CT26/mβG-eB7 and the CT26 tumor images with contrast agent [Gd(DOTA-FPβG)] due to perfusion and extracellular environments is therefore unlikely.

The average signal intensity of liver tissues in the MRI scan with [Gd(DOTA-FPβG)] and $[Gd(DOTA)]^-$ is higher than the signal intensity of CT26 tumors 5 minutes after injection, and then it decreases rapidly. The fast-increasing and decaying trend of signal strength of the liver is due to high blood perfusion in the liver tissues. The contrast media in the serum are excreted rapidly by the kidney. The liver tissues remain with just a small amount of contrast media in extracellular spaces. The signal intensity of liver reduces quickly and becomes ever closer to the signal intensity of CT26 tumors.

MRI can be performed successfully in large animals and humans without limitation of penetration in optical imaging. It also shows the images with better spatial resolution than those from modalities of nuclear medicine.

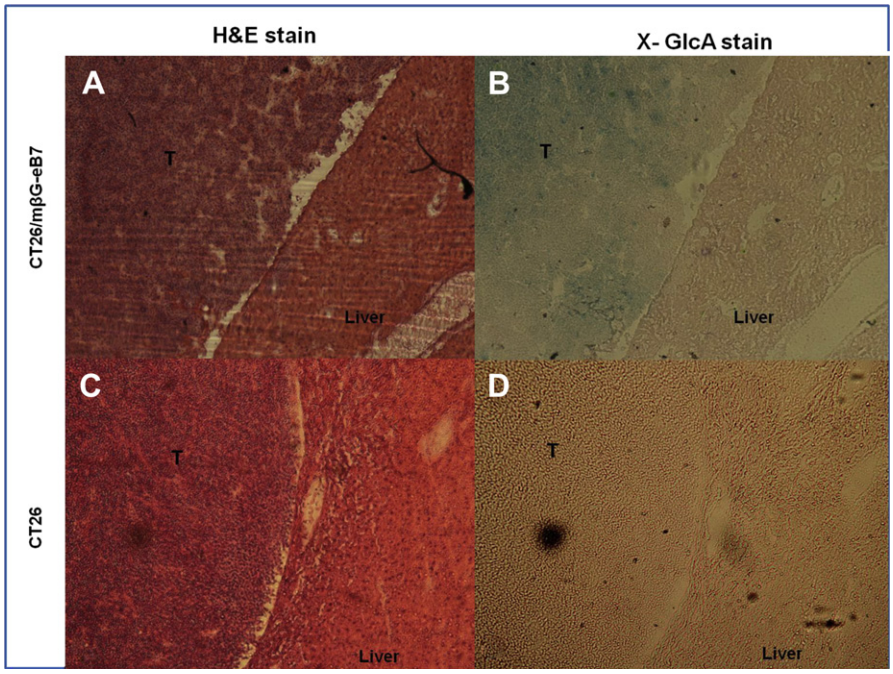

Figure 8. Histology demonstrates CT26/mβG-eB7 tumor (T = tumor), CT26 tumor and liver tissues stained by hematoxylin and eosin (A, C), and X- GlcA (B, D). The area of CT26/mβG-eB7 tumor reveals blue stain (B) because of βG expression. The CT26 tumor reveals no blue stain (D).

Therefore, MRI is more clinically transferrable from preclinical evaluation to real clinical scenarios. There are other commercial contrast media [18,24,25], e.g., Gd-EOB-DTPA (Primovist, Bayer, Germany) [26—29], Gd-BOPTA (MultiHance, Bracco, Italy) [30—32], and ferucarbotran (Resovist, Bayer, Germany) [32—34], which have certain affinity to receptors of hepatocyte or Kupffer cell. However, they do not target tumor cells directly. Just which agent in which scanning parameters can detect tumors more accurately than the others is still to be determined. More studies are required to compare different imaging strategies for detecting tumors with MRI.

There are limitations to the approach we used in the study. The βG enzyme does not exist in all membranes of tumor cells. Some researchers point out that βG was one of the often-expressed biomarkers on many tumor membranes. The contrast medium [Gd(DOTA-FPβG)] can be applied to detect whether the tumor expresses βG enzyme. Many oncologic studies try to detect special biomarkers and administer chemotherapy with tumor-specific or sensitive prodrugs for tumor treatment [35]. These prodrugs may have a high affinity with tumors and may be activated by the enzyme in tumor cells. Due to its better tumor affinity, the dosage and toxicity of patients can be reduced without compromising the treatment effect. Molecular imaging, such as our design in this experiment, may also play a role in management of oncologic patients in the future.

In conclusion, we confirm that better contrast enhancement can be readily detected *in vivo* by use of a tissue-specific MRI contrast agent targeting tumor cells with specific biomarkers in a clinical MRI scanner. Molecular imaging strategy can expand to a more clinically feasible imaging modality as long as tissue-specific contrast agents can be successfully synthesized and safely administered.

Acknowledgments

This research was supported by a grant (97-2314-B-037-038-MY3) from the National Science Council of Taiwan.

References

[1] Haradome H, Grazioli L, Tinti R, Morone M, Motosugi U, Sano K, et al. Additional value of gadoxetic acid-DTPA-enhanced hepatobiliary phase MR imaging in the diagnosis of early-stage hepatocellular carcinoma: comparison with dynamic triple-phase multidetector CT imaging. J Magn Reson Imaging 2011;34:69—78.

[2] Khan AS, Hussain HK, Johnson TD, Weadock WJ, Pelletier SJ, Marrero JA. Value of delayed hypointensity and delayed enhancing rim in magnetic resonance imaging diagnosis of small hepatocellular carcinoma in the cirrhotic liver. J Magn Reson Imaging 2010;32:360—6.

[3] Park Y, Kim Y, Lee JH, Lee EY, Kim HS. Usefulness of serum anti-p53 antibody assay for lung cancer diagnosis. Arch Pathol Lab Med 2011;135:1570—5.

[4] Moore RG, Miller MC, Disilvestro P, Landrum LM, Gajewski W, Ball JJ, et al. Evaluation of the diagnostic accuracy of the risk of ovarian malignancy algorithm in women with a pelvic mass. Obstet Gynecol 2011;118:280—8.

[5] Misteli T, Spector DL. Applications of the green fluorescent protein in cell biology and biotechnology. Nat Biotechnol 1997;15:961—4.

[6] Yang M, Baranov E, Jiang P, Sun FX, Li XM, Li L, et al. Whole-body optical imaging of green fluorescent protein-expressing tumors and metastases. Proc Natl Acad Sci U S A 2000;97:1206—11.

[7] Liang Q, Nguyen K, Satyamurthy N, Barrio JR, Phelps ME, Gambhir SS, et al. Monitoring adenoviral DNA delivery, using a mutant herpes simplex virus type 1 thymidine kinase gene as a PET reporter gene. Gene Ther 2002;9:1659—66.

[8] Yu J, Liu L, Kodibagkar VD, Cui W, Mason RP. Synthesis and evaluation of novel enhanced gene reporter molecules: detection of beta-galactosidase activity using ^{19}F NMR of trifluoromethylated aryl beta-D-galactopyranosides. Bioorg Med Chem 2006;14:326—33.

[9] Aleksandrowicz J, Starek A, Moszczynski P, Czarnobilski Z. [Changes in the activity of lysosome beta-glucuronidase in rat leukocytes treated with various doses of selenium]. Patol Pol 1978;29:143—51.

[10] de Graaf M, Boven E, Scheeren HW, Haisma HJ, Pinedo HM. Beta-glucuronidase-mediated drug release. Curr Pharm Des 2002;8:1391—403.

[11] Boyer MJ, Tannock IF. Lysosomes, lysosomal enzymes, and cancer. Adv Cancer Res 1993;60:269—91.

[12] Colin M, Moritz S, Schneider H, Capeau J, Coutelle C, Brahimi-Horn MC. Haemoglobin interferes with the ex vivo luciferase luminescence assay: consequence for detection of luciferase reporter gene expression *in vivo*. Gene Ther 2000;7:1333—6.

[13] Su YC, Chuang KH, Wang YM, Cheng CM, Lin SR, Wang JY, et al. Gene expression imaging by enzymatic catalysis of a fluorescent probe via membrane-anchored beta-glucuronidase. Gene Ther 2007;14:565—74.

[14] Antunes IF, Haisma HJ, Elsinga PH, Dierckx RA, de Vries EF. Synthesis and evaluation of [18F]-FEAnGA as a PET Tracer for beta-glucuronidase activity. Bioconjug Chem 2010;21:911—20.

[15] Klutz K, Willhauck MJ, Dohmen C, Wunderlich N, Knoop K, Zach C, et al. Image-guided tumor-selective radioiodine therapy of liver cancer after systemic nonviral delivery of the sodium iodide symporter gene. Hum Gene Ther 2011;22:1563—74.

[16] Shirai S, Sato M, Suwa K, Kishi K, Shimono C, Kawai N, et al. Single photon emission computed tomography-based three-dimensional conformal radiotherapy for hepatocellular carcinoma with portal vein tumor thrombus. Int J Radiat Oncol Biol Phys 2009;73:824—31.

[17] Wang D, Jin B, Lewandowski RJ, Ryu RK, Sato KT, Mulcahy MF, et al. Quantitative 4D transcatheter intraarterial perfusion MRI for monitoring chemoembolization of hepatocellular carcinoma. J Magn Reson Imaging 2010;31:1106—16.

[18] Nishie A, Tajima T, Ishigami K, Ushijima Y, Okamoto D, Hirakawa M, et al. Detection of hepatocellular carcinoma (HCC) using super paramagnetic iron oxide (SPIO)-enhanced MRI: added value of diffusion-weighted imaging (DWI). J Magn Reson Imaging 2010;31:373—82.

[19] Whittaker S, Marais R, Zhu AX. The role of signaling pathways in the development and treatment of hepatocellular carcinoma. Oncogene 2010;29:4989—5005.

[20] Baffy G, Brunt EM, Caldwell SH. Hepatocellular carcinoma in nonalcoholic fatty liver disease: an emerging menace. J Hepatol 2012;56:1384—91.

[21] Colli A, Fraquelli M, Casazza G, Massironi S, Colucci A, Conte D, et al. Accuracy of ultrasonography, spiral CT, magnetic resonance, and alpha-fetoprotein in diagnosing hepatocellular carcinoma: a systematic review. Am J Gastroenterol 2006;101:513—23.

[22] Yu NC, Chaudhari V, Raman SS, Lassman C, Tong MJ, Busuttil RW, et al. CT and MRI improve detection of

hepatocellular carcinoma, compared with ultrasound alone, in patients with cirrhosis. Clin Gastroenterol Hepatol 2011;9: 161—7.
[23] Chang YT, Cheng CM, Su YZ, Lee WT, Hsu JS, Liu GC, et al. Synthesis and characterization of a new bioactivated paramagnetic gadolinium(III) complex [Gd(DOTA-FPG)(H_2O)] for tracing gene expression. Bioconjug Chem 2007;18:1716—27.
[24] Abdullah SS, Pialat JB, Wiart M, Duboeuf F, Mabrut JY, Bancel B, et al. Characterization of hepatocellular carcinoma and colorectal liver metastasis by means of perfusion MRI. J Magn Reson Imaging 2008;28:390—5.
[25] Hsu JS, Jaw TS, Liu GC, Wang YM, Chen SH, Kuo YT, et al. Evaluation of $[Gd(Bz\text{-}TTDA)]^{2-}$ as a potential contrast agent in MR imaging of the hepatobiliary system: an animal study. J Magn Reson Imaging 2004;20:632—9.
[26] Kunishi Y, Numata K, Morimoto M, Okada M, Kaneko T, Maeda S, et al. Efficacy of fusion imaging combining sonography and hepatobiliary phase MRI with Gd-EOB-DTPA to detect small hepatocellular carcinoma. AJR Am J Roentgenol 2012;198:106—14.
[27] Lee S, Kim SH, Park CK, Kim YS, Lee WJ, Lim HK. Comparison between areas with Gd-EOB-DTPA uptake and without in hepatocellular carcinomas on Gd-EOB-DTPA-enhanced hepatobiliary-phase MR imaging: pathological correlation. J Magn Reson Imaging 2010;32:719—25.
[28] Saito K, Araki Y, Park J, Metoki R, Katsuyama H, Nishio R, et al. Effect of Gd-EOB-DTPA on T2-weighted and diffusion-weighted images for the diagnosis of hepatocellular carcinoma. J Magn Reson Imaging 2010;32:229—34.
[29] Motosugi U, Ichikawa T, Sou H, Sano K, Ichikawa S, Tominaga L, et al. Dilution method of gadolinium ethoxybenzyl diethylenetriaminepentaacetic acid (Gd-EOB-DTPA)-enhanced magnetic resonance imaging (MRI). J Magn Reson Imaging 2009;30:849—54.
[30] Kreft BP, Tanimoto A, Stark DD, Baba Y, Zhao L, Chen JT, et al. Enhancement of tumor-liver contrast-to-noise ratio with gadobenate dimeglumine in MR imaging of rats. J Magn Reson Imaging 1993;3:41—9.
[31] Manfredi R, Maresca G, Baron RL, Cotroneo AR, De Gaetano AM, De Franco A, et al. Delayed MR imaging of hepatocellular carcinoma enhanced by gadobenate dimeglumine (Gd-BOPTA). J Magn Reson Imaging 1999;9:704—10.
[32] Kim YK, Kim CS, Kwak HS, Lee JM. Three-dimensional dynamic liver MR imaging using sensitivity encoding for detection of hepatocellular carcinomas: comparison with superparamagnetic iron oxide-enhanced mr imaging. J Magn Reson Imaging 2004;20:826—37.
[33] Okada M, Imai Y, Kim T, Kogita S, Takamura M, Kumano S, et al. Comparison of enhancement patterns of histologically confirmed hepatocellular carcinoma between gadoxetate- and ferucarbotran-enhanced magnetic resonance imaging. J Magn Reson Imaging 2010;32:903—13.
[34] Ishiyama K, Hashimoto M, Izumi J, Watarai J, Shibata S, Sato T, et al. Tumor-liver contrast and subjective tumor conspicuity of respiratory-triggered T2-weighted fast spin-echo sequence compared with T2*-weighted gradient recalled-echo sequence for ferucarbotran-enhanced magnetic resonance imaging of hepatic malignant tumors. J Magn Reson Imaging 2008;27:1322—6.
[35] Cho EJ, Yang J, Mohamedali KA, Lim EK, Kim EJ, Farhangfar CJ, et al. Sensitive angiogenesis imaging of orthotopic bladder tumors in mice using a selective magnetic resonance imaging contrast agent containing VEGF121/rGel. Invest Radiol 2011;46:441—9.